Optimized design of doubly salient permanent magnet generator taking into account the efficiency of energy conversion

Nacereddine Harkati[1], **Luc Moreau**[1], **Jean-Frédéric Charpentier**[2], **Mohammed El Hadi Zaïm**[1]

1. Laboratoire IREENA, Polytech Nantes., Université de Nantes
BP 406, 44602 Saint-Nazaire, France
el-hadi.zaim@univ-nantes.fr

2. Laboratoire IRENav, Ecole Navale, 29240 Brest, France
jean-frederic.charpentier@ecole-navale.fr

ABSTRACT. *This paper presents a design methodology of a doubly salient PM generator to be associated to a tidal stream turbine. The behavior and the supply strategy of this unconventional machine are firstly described. An energy ratio and a torque to mass ratio are defined as two criteria to optimize for the design of such system. In fact these criteria are related to systems compactness and converter sizing. A simple method for the calculations of these two criterions is proposed. The influence of the variation of the main geometrical parameters which define the machine geometry on these criteria are firstly studied. Then a multi-objective optimization process is used to optimize these two design criteria. From the calculations of 20,000 set of machine configurations, a Pareto front is highlighted. Typical points of this Pareto front which corresponds to several DSPM designs are analyzed. The results highlight the interest of proposed method.*

RÉSUMÉ. *Cet article présente une méthodologie de conception d'une génératrice à aimants permanents doublement saillante pour hydrolienne. Le comportement et la stratégie de contrôle de cette machine non conventionnelle sont décrits. Un ratio d'énergie et un rapport de couple massique sont définis pour optimiser à la fois la compacité du générateur et le dimensionnement du convertisseur. Une méthode simple pour les calculs de ces deux critères est proposée. Les influences des principaux paramètres géométriques de la machine sur ces critères sont étudiées. Ensuite, un processus d'optimisation multi-objectifs est utilisé. À partir des calculs de ces critères pour 20 000 paramètres géométriques, un front de Pareto concernant les deux critères d'optimisation est mis en évidence. Plusieurs points caractéristiques de ce front de Pareto qui correspondent à des dimensionnements différents sont présentés et analysés. Les résultats mettent en évidence l'intérêt de la méthode proposée.*

KEYWORDS: *design optimization, doubly salient, dspm; energy ratio, low speed, permanent magnet generators.*

MOTS-CLÉS: *Conception de machines électriques, machines spéciales, faible vitesse, génératrices à aimants permanents, hydrolienne.*

DOI:10.3166/EJEE.18.319-338 © Lavoisier 2016

1. Introduction

Different low-speed high-torque structures have been investigated for the energy production application (Benelghali *et al.*, 2007; Benelghali *et al.*, 2012; Keysan *et al.*, 2011; Pinilla, 2011 ; Wang *et al.*, 2011). Indeed, the direct-drive allows to remove or to simplify the gearbox and so to reduce the maintenance of the system.

Among these structures, new robust structures having both magnets and windings in the stator have been studied in the two last decades (Chau *et al.*, 2005; Dinyu *et al.*, 1999; Ming *et al.*, 2001a, 2001b, 2001c; Wang *et al.*, 2001; Wei *et al.*, 2008; Ying *et al.*, 2006, 2009; Yu *et al.*, 2012; Yuefeng *et al.*, 1995).

This paper focuses on such an unconventional low speed PM generator which uses a passive rotor. The absence of magnetic sources in the rotor reduces the thermal stresses because losses are mainly located in the stator which is easier to cool. So this generator can be an interesting alternative for direct drive systems and can fit the tidal energy specifications and constraints (Harkati *et al.*, 2013).

The objective of the paper is to optimize the design of the proposed structure considering constraints related to the sizing of the power converter. First, the generator structure is presented. Next, the design criterions and operating principle for a giving supply are shown. Finally, an optimization process based on a finite element analysis is proposed, which allows to define a set of optimum geometrical parameters for the structure.

2. Generator description

The proposed generator is based on reluctance machine and uses magnets located on the stator yoke. This structure is known as “Doubly Salient Permanent Magnet” (DSPM) (Chau *et al.*, 2005; Dinyu *et al.*, 1999; Ming *et al.*, 2001a, 2001b, 2001c; Ying *et al.*, 2006; 2009; Yuefeng *et al.*, 1995). The structure is salient in both the stator and the rotor. The rotor consists of a simple stack of laminations with Nr=64 small teeth. Four Nd-Fe-B magnets are housed in the stator yoke which has Ns =48 small teethes located in 12 more large teeth. The machine has then pa=2 pole pairs relative to the coil winding and pe=2 pole pairs relative to the excitation circuit (magnets). Nr, Ns, pa and pe must fulfill the following condition (Rezzoug *et al.*, 2011) :

$$\pm N_r \pm N_s = \pm k_1 p_a \pm k_2 p_e \quad (1)$$

where k_1 and k_2 are integers.

The general topology of the studied machine is shown in Figure 1. The permanent magnets provide a flux concentration in the air gap and the 3-phases stator windings are concentrated around the stator large teeth.

The specificity of the proposed DSPM compared to other DSPM found in literature is that it includes large toothed teeth which allow the increasing of the number of rotor teeth leading to the increase of the electrical frequency. Indeed the rotor speed varies inversely with number rotor teeth; it is why this kind of machine can operate at low speed with only a small number of magnets and coils (Rezzoug *et al.*, 2011). Note that all teeth in one pole are magnetically polarized with a single winding.

This is why this DSPM is characterized by a simple structure, low cost and high mass to torque ratio. In addition, all active parts are in stator.

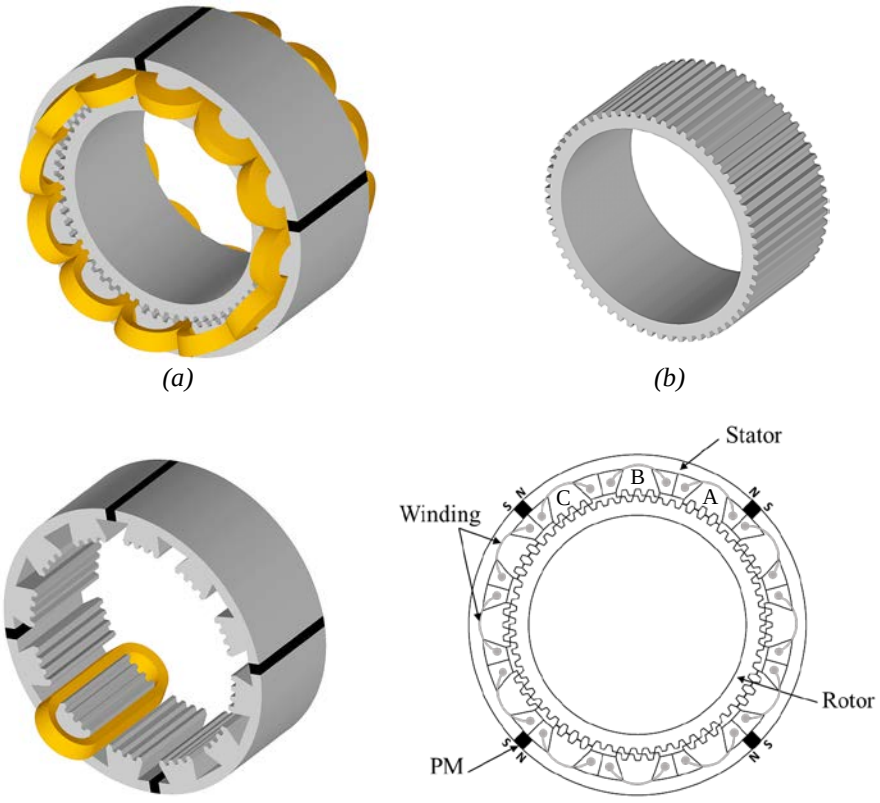

Figure 1. (a) Complete structure of DSPM generator (b) Passive rotor (c) Stator with one concentric winding (d) Cross section of DSPM

3. Operating principle and design criterions

3.1. Operating principle

Figure 2 illustrates the basic operating principle of the machine. As for classical switched reluctance machine, an ideal rectangular current supply controlled according to the position by a PWM converter is considered. Current is positive in each phase when the PM flux decreases ($\partial\psi_{PM}/\partial\theta<0$) over 120° of the electrical period. In this case the total EM torque (which is negative in generator mode) can be obtained by the superposition of the 3 phase's statics torques. It can be noticed with this supply strategy, only one phase is supplied at any time. It is why the behaviour of the machine with only one phase supplied allows to estimate the global behaviour of the system.

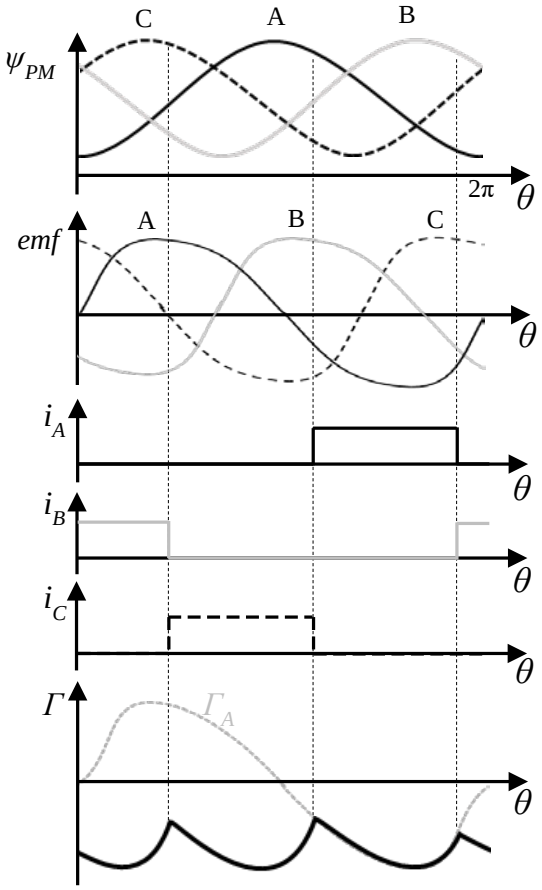

Figure 2. Operating principle of the DSPM

3.2. Design criterions

Because of complex geometry and high saturation effects in the machine, numerical simulations are used for accurate electromagnetic characteristics prediction.

Figure 3 presents the curves flux vs. current (ψ(i)) in one phase for two specific positions of the rotor (conjunction (AB curve) and opposition (EC curve)). The current varies from 0 to its rated value (in p.u). The opposition position corresponds to a maximum global air gap for the corresponding supplied phase and a minimal flux. In this position the flux varies almost linearly with the current. Another specific position is when the rotor and stator teeth of one phase are aligned. This position is called position of conjunction and corresponds to a minimal air gap and maximal flux. Because of a smaller air gap, magnetic saturation appears at this position. This is why the EC curve is not linear. The operating cycle of the machine per phase on an electrical period could be described in the plane ψ(i) by an energy cycle. The ABCD area (R+W) represents the maximum total energy involved in the machine-converter assembly. This maximum value of the total energy is directly related to the maximum apparent power of the converter (Miller, 1993). The area ABCE (W) between the two curves of opposition position and conjunction position represents the maximum energy available for electromechanical conversion per cycle. In real operation, only a part of this energy can be used.

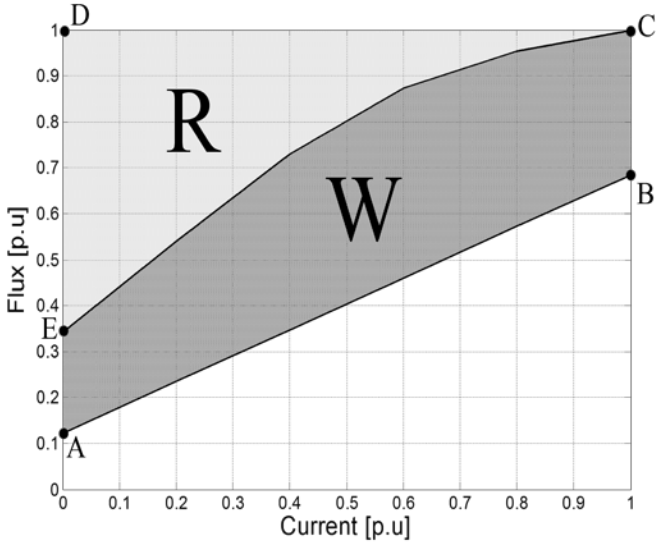

Figure 3. Flux vs. current characteristics for 2 particular positions (AB opposition and CE conjunction)

During the energy conversion, the ratio between the energy which can be used for electromechanical conversion and the total energy exchanged with the converter considerably affects to the efficiency of energy conversion, it depends on the shape of the flux vs. current characteristics (ψ,i) for the two particular rotor positions.

The ratio of energy noted λ is introduced by (Lawrenson *et al.*, 1980) and (Miller, 1985) and defined as:

$$\lambda = \frac{W}{W+R} \tag{2}$$

This ratio is classically used in variable speed switched reluctance motor to evaluate the impact on the machine design on the converter sizing. The value of λ gives an idea on the rated power of the converter in comparison with the rated power of the generator. More λ is high; more the rated power of the converter is close to the rated power of the machine. A low λ results in an oversizing of the converter. This is why an improvement of this ratio results in decreasing the size of the converter (Miller, 1993). We extend it in this work to the excited machine.

The calculation of the torque is based on the virtual work method. The torque value can be obtained by deriving the magnetic . with a constant current when the angular position varies. The average torque can be estimated from the energy cycle from the knowledge of the co-energy on the two previously defined specific positions (conjunction and opposition). An energy cycle is defined for an electrical period. So in a mechanical turn, each phase of the DSPM sees N_r =64 energy cycles. The average torque can be approximated as:

$$\Gamma_{av} = \frac{N_r W}{2\pi} \tag{3}$$

To increase the efficiency of energy conversion, the machine design will be sized and optimized in order to increase the energy ratio and the mass to torque ratio. This optimization process is described in the next section.

4. DSPM design optimization taking into account converter constraints

The aim of this part is to optimize both mass to torque ratio (Sadowski *et al.*, 1992) and a criterion related to the sizing of the power converter. This is why the goal of the design procedure is to improve the energy ratio while seeking a maximum mass to torque ratio. This latter is equal to the average torque divided by the total active mass of the structure. To achieve these objectives, the diagram described in Figure 3 is used to calculate both average torque and energy ratio values. These calculations require only the determination of the two flux vs. current curves, corresponding to opposition and conjunction position for a single phase supplied by a variable constant current. Mutual coupling between phases are neglected considering the supply strategy described in previous section. In fact the

overlapping phases between the phase supply corresponding to current increase and decrease are neglected. For each set of optimization variables, these two flux vs. current curves are determined using magneto-static Finite Element (FE) field calculations taking into account saturation effects. These calculations allow determining the flux for several values of the phase current for the two positions. Because of the symmetries of the DSPM structure, only 1/8th of the structure is modeled in the FE process.

The used optimization variables are 13 geometric parameters defining the DSPM structure. These parameters are shown in Figure 4.

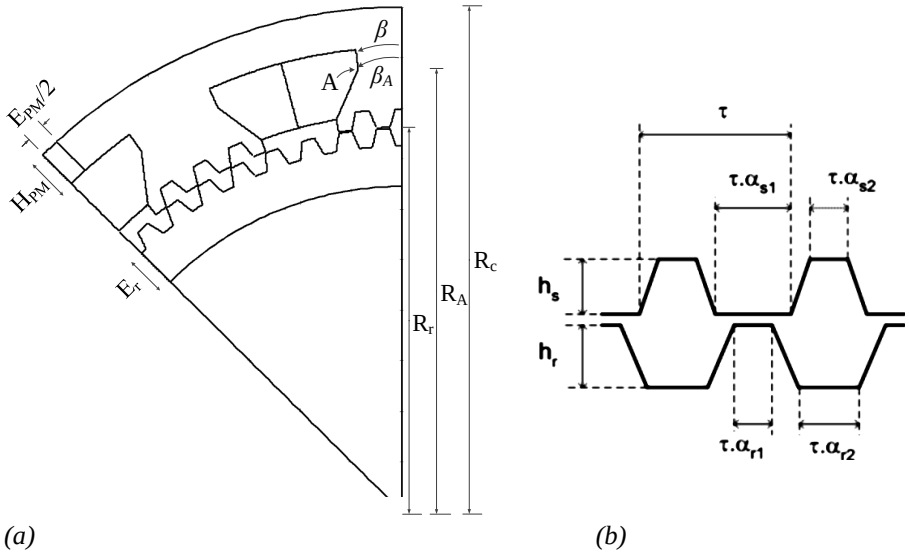

Figure 4. (a) Main DSPM geometry dimensions
(b) Teeth shape dimensions

– Teeth cyclic ratios α_{r1}, α_{s1}, α_{r2} and α_{s2}

– Rotor and stator teeth height h_s and h_r

– Magnet thickness and height E_{PM} and H_{PM}

– Rotor yoke thicknesses E_r

– Slot opening angle β

– Point A coordinates defined by (R_A, β_A)

– Core radius R_r

Constraints and bounds on these variables are defined in Table 1. These common data corresponds to the specifications of small-scale generator used for laboratory experiments.

Table 1. Dimensions constraints

$4mm \leq (h_s, h_r) \leq 12mm$
$0.2 \leq (\alpha_{r1}, \alpha_{s1}, \alpha_{r2}, \alpha_{s2}) \leq 0.5$
$6mm \leq E_{PM} \leq 26mm$
$5mm \leq (H_{PM}, E_r) \leq 30mm$
$150mm \leq R_r \leq 160mm$
$155mm \leq R_A \leq 170mm$
$1° \leq (\beta, \beta_A) \leq 15°$

Common data are used for all the studied cases. Neodymium rare earth magnets are used with a magnetization $B_r=1.17T$. The rotor and stator cores are made of M400-50A material (Saou *et al.*, 2008). The copper coils are placed into the stator slots. To insure a convenient cooling, current maximal density in the coils is fixed at $5A/mm^2$ with a slot fill factor $k_r=0.5$ for all simulations.

4.1. Parametric analysis

Firstly, the study aims to identify the influence of each geometric parameter of the DSPM separately on the evaluation of the mass to torque ratio and energy ratio.

This first parametric analysis requires a reference structure (only one parameter varies and the other parameters are equal to those of the reference machine). Table 2 shows the detail of the geometric parameters of the reference structure named "DSPM0". This reference structure corresponds to a first design established in previous work which corresponds to a generator designed for a low power laboratory scale experimental turbine (Harkati *et al.*, 2013). The rotor and the stator of this structure are shown in Figure 5 and its characteristics are presented in Table 3.

In order to normalize results, all parameters quantities are given in per unit (p.u) from this reference design. The DSPM0 torque to mass ratio and energy ratio are equal to $\Gamma_{mass0} = 6.39$ N.m/kg and $\lambda_0 = 0.59$ respectively.

Table 2. Reference structure dimensions

Symbol	Quantity	Value
long	Length	150 mm
R_c	Outer radius	200 mm
e	Air gap	0,5 mm
R_r	Core radius	152 mm
E_r	Rotor yoke thickness	16 mm

α_s ; h_s	Small teeth stator parameters	0,35; 7mm
α_r ; h_r	Small teeth rotor parameters	0,35 ; 7mm
H_{PM}	Height of the magnets	16mm
E_{PM}	Width of the magnets	15mm

Table 3. Reference structure (DSPM0) characteristics

Symbol	Quantity	Value
P	Power	2 kW
Ω	Speed	50 rpm
N_{spires}	Number of turns per coil	160
J_s	Current density	5 A/mm²
k_r	Slot fill factor	0.5
B_r	PM magnetization	1,17 T
μ_{PM}	PM relative permeability	1.089

Figure 5. Reference Prototype (DSPM0) stator and rotor cores

4.1.1. Influence of the shape of trapezoidal teeth

This part consists in studying the effect of the geometry variation of the small teeth while keeping the other geometric parameters equal to those of the reference structure “DSPM0”. The influence of the height and width of the teeth is studied.

Figure 6 shows the energy ratio λ and torque to mass ratio Γ_{mass} evolutions with the same shape of teeth in the stator and the rotor ($\alpha_{s1}=\alpha_{s2}=\alpha_{r1}=\alpha_{r2}=\alpha$ and $h_s=h_r=h$) when the teeth cyclic ratio varies (Figure 6a) and when the teeth height varies (Figure 6b). The teeth pitch angle ($\tau=2\pi/N_r$) is maintained constant.

The presence of the magnetic saturation affects the shape of the (ψ, i) characteristics, and affects the energy ratio.

The torque of the DSPM depends on two effects: saliency and saturation effects. For small value of *h*, the more teeth are deep, the more the saliency effects are important and lead to increase the torque (Figure 6b). This profit obtained by the saliency will be counteracted by the high level of saturation for high value of *h*. These two effects lead to a maximum torque as observed in Figure 6b.

In this case, the values $\alpha=0.35$ and $h=0.07$ retained in the reference structure is not too far from the optimum results both in terms of torque to mass ratio or in terms of energy ratio.

4.1.2. Influence of magnets dimensions

In this part the effect of the magnet thickness and height is analyzed. When the magnet height varies at fixed external radius, the same height for all the slots is maintained as a constant by varying the core radius. That means that the copper section is maintained as a constant for all the studied cases.

Increasing H_{PM} will increase the effective area of the magnets; therefore it will create a higher magnetic flux which requires bigger rotor yoke thickness to limit the saturation effects in the rotor. This rotor yoke thickness is fixed to be equal to the stator yoke thickness ($E_r=H_{PM}$). All other dimensions are set to their reference values.

Figure 7a presents the evolution of the torque to mass ratio and the energy ratio when the magnet height varies. It can be noticed that for small values of magnet height, Γ_{mass}, increases with H_{PM} because the flux of the magnets increases for the same current. Too high values of H_{PM} results in high level of saturation in the machine teeth and leads to lower values of the torque to mass ratio. The energy ratio λ increases with magnet height because the relative part of the total flux in the machine which is created by the magnet increases.

Considering the variation of the magnet thickness E_{PM} (Figure 7b), the volume of magnets can be multiplied by more than 4 without having a significant effect neither on the mass to torque ratio nor on the energy ratio. These two criterions remain quasi constants (±0.5%). Indeed the increase of magnet thickness is counterbalanced by the increase of the reluctance of the magnetic circuit because the PM relative permeability is near of 1. So choosing small values of the PM thickness seems to be more advantageous.

However it can be noticed that magnet dimensions has also to be fixed considering demagnetization constraints. In the worst case of supply, the magnet field in the magnet must be greater than the coercive field of the magnet material to avoid demagnetization effects.

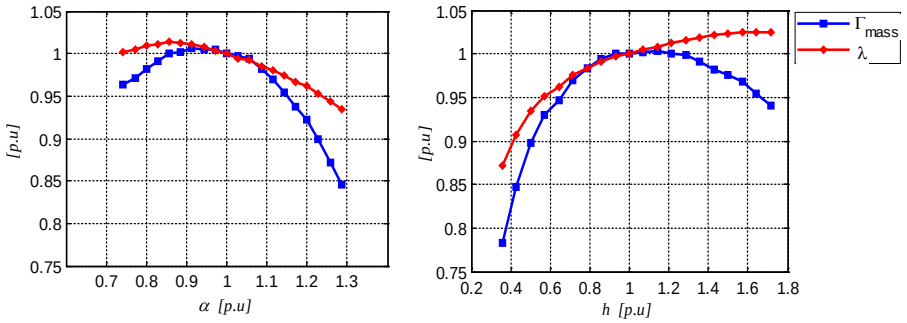

(a) *(b)*

Figure 6. Influence of variation of the form of trapezoidal teeth on torque to mass ratio and energy ratio (p.u. reference values corresponds to DSPM0 design and $\alpha_{s1}=\alpha_{s2}=\alpha_{r1}=\alpha_{r2}=\alpha$ and $h_s=h_r=h$)

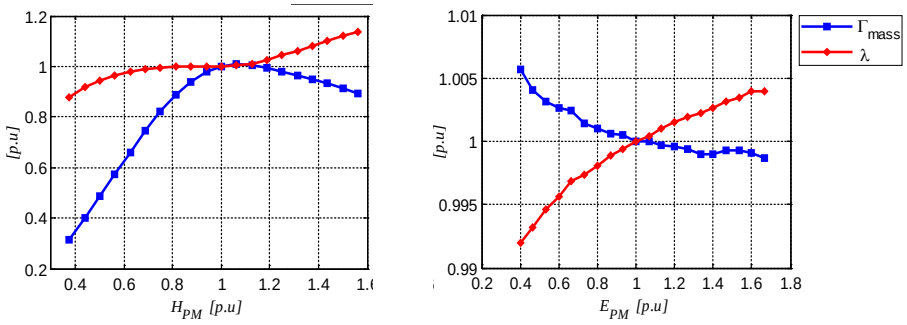

(a) *(b)*

Figure 7. Influence of variation of magnets dimensions on torque to mass ratio and energy ratio (p.u. reference values corresponds to DSPM0 design)

4.1.3. Influence of slot opening angle

Figure 8 presents the variation of the energy ratio λ and torque to mass ratio when the opening of the slot defined by the angle β varies between 0.65 to 1.6 p.u. This variation relates to a change in the space available for the winding (more β is high, more the slot area decreases). The energy ratio varies slightly (the slight decrease of λ can be explained by the saturation effect on the ψ(i) characteristics). However the opening of the slot has a direct impact on the torque to mass ratio. If β increases, in one hand, it leads to decreasing the saturation level in the magnetic circuit, in the other hand it leads also to decreasing the machine electric load. A compromise can be found between these two contradictory effects which corresponds to β=0.8 p.u for the reference dimensions.

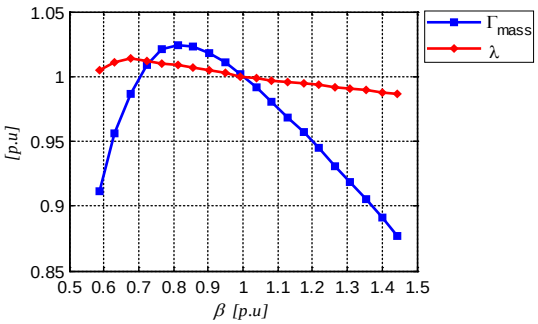

Figure 8. Influence of variation of slot opening angle on torque to mass ratio and energy ratio (p.u. reference values corresponds to DSPM0 design)

4.2. Global optimization

In a second step, a global optimization procedure based on a systematic approach (systematic variation of the dimensions in the range defined in Table 1) is used in order to determine for a fixed global volume (external radius and length are fixed) the combinations of the 13 parameters which give the highest energy ratio and the highest torque to mass ratio.

The optimization problem is written in the form of a MATLAB program that associated to FEMM software for the finite element electromagnetic analysis. The block diagram (Figure 9) describes the procedure followed.

Optimisation variables: $X = (\alpha_{r1}, \alpha_{s1}, \alpha_{r2}, \alpha_{s2}, h_s, h_r, E_{PM}, H_{PM}, E_r, \beta, R_A, \beta_A, R_r)$

Variable bounds: $X_{min} = [0.2, 0.2, 0.2, 0.2, 4, 4, 6, 5, 5, 1, 155, 1, 150]$
$X_{max} = [0.5, 0.5, 0.5, 0.5, 12, 12, 26, 30, 30, 15, 170, 15, 160]$

Optimization objective functions: min $(-\Gamma_{mass}(X), -\lambda(X))$

Figure 10 shows the energy ratio and mass to torque ratio for 20,000 DSPM configurations with different geometries. These values have been obtained using finite element analysis by the same method described in previous sections. These results allow to underline the Pareto front shown in Figure 9 with green points.

When the same shape and dimensions of the stator and rotor teeth are chosen to be identical ($\alpha_{s1}=\alpha_{r1}$; $\alpha_{r2}=\alpha_{s2}$ *and* $h_s=h_r=h$), the number of optimization variables can be reduced to 9. The Pareto front is then given by the red points in Figure 10.

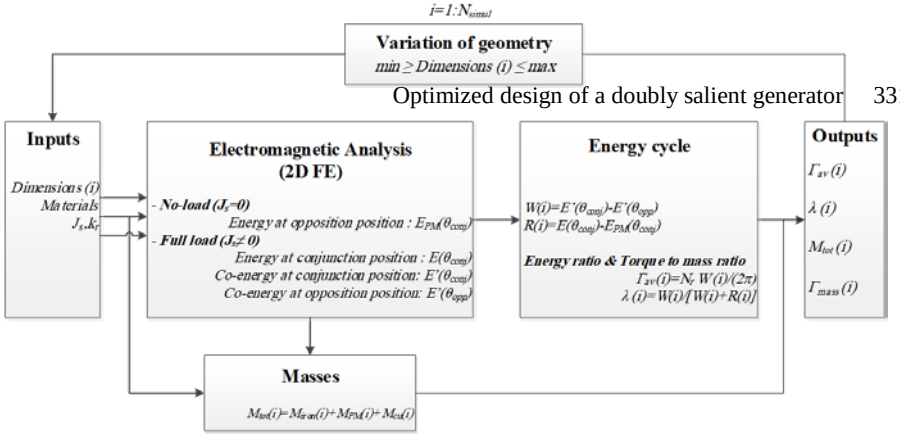

Figure 9. Procedure of optimization

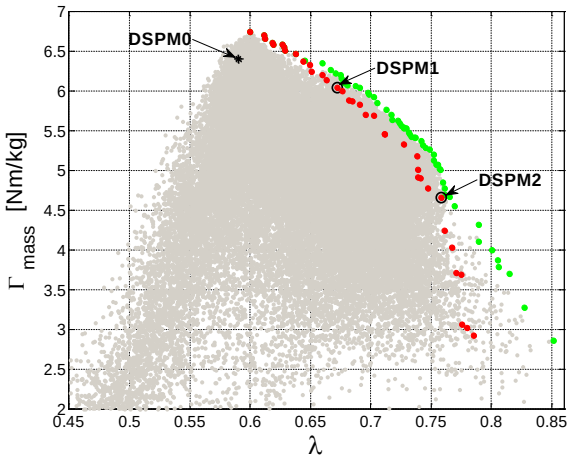

Figure 10. Optimisation results: mass to torque ratio VS Energy ratio

Two typical configurations of the DSPM structure are considered in this last Pareto fronts and compared with the reference configuration DSPM0 (Figure 11).

– The DSPM0 is the reference machine previously designed. This structure is characterized by $\Gamma_{mass0}=6.39$ *N.m/kg* and an energy ratio of $\lambda_0=0.59$.

– The DSPM1 has a mass to torque ratio close to the one of the DSPM0 ($\Gamma_{mass1}=6.04$ *N.m/kg*), but its energy ratio is improved by 14% ($\lambda_1=0.67$).

– The DSPM2 is characterized by an energy ratio 29% higher than that of DSPM0 ($\lambda_2=0.76$), and a mass to torque ratio 27% smaller ($\Gamma_{mass2}=4.66$ *N.m/kg*).

Tables 4 and 5 summarize respectively the geometrical dimensions and the characteristics of the 3 selected configurations.

A schematic view of these 3 machines is represented at Figure 11. Dashed lines in Figure 11b and 11c present the DSPM0 geometry.

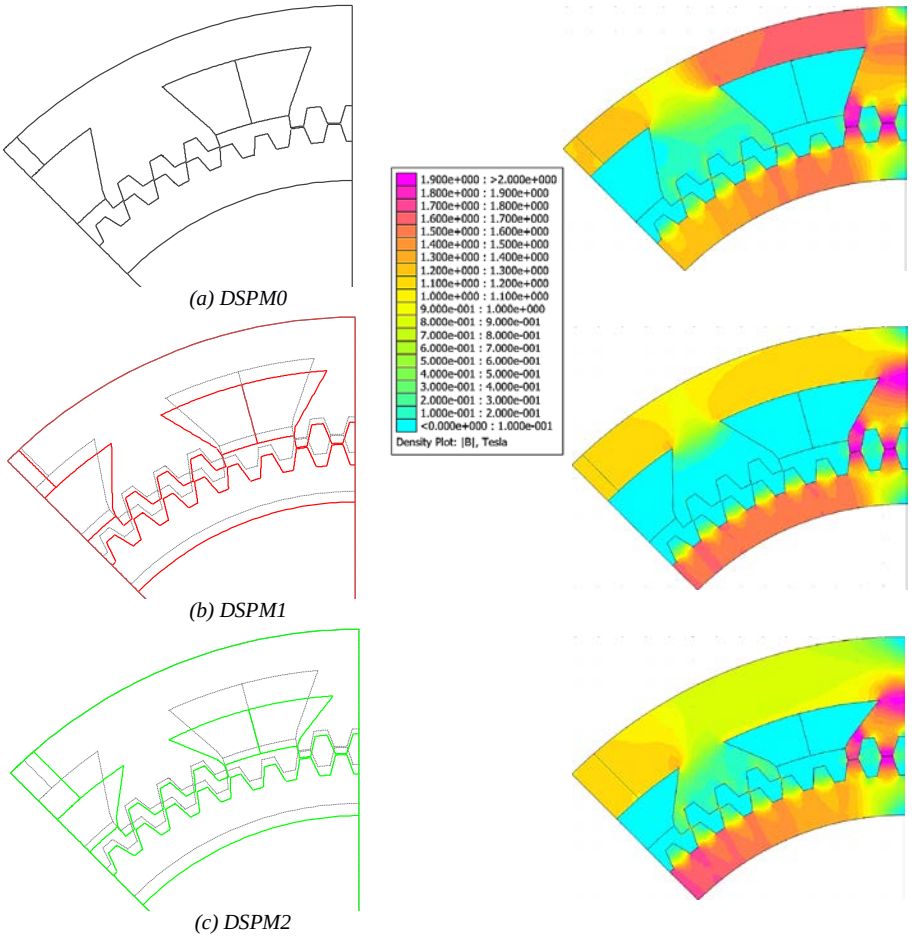

(a) DSPM0

(b) DSPM1

(c) DSPM2

Figure 11. Configurations retained for the comparison
Magnetic flux density distribution at full load for the conjunction position of the phase B

Finite element analysis allows to evaluate the back-EMF at no-load, the self-inductance and the static torque at full load of the 3 machines. These values are achieved by varying the position of the rotor on an electrical period corresponding to a mechanical angle of 5.625 degrees.

Figure 11 shows the flux density distribution in the 3 configurations at full load for the conjunction position of the phase B. These maps give a view of the magnetic state of the 3 structures, to identify the most affected locations by the magnetic saturation. The maximal values of the flux density are around 1.6 to 1.9T in the teeth in conjunction and also on some areas in the stator and rotor yokes. According to the

characteristic B(H) of the used laminations (Saou *et al.*, 2008), these flux density values lead to high saturation of these parts of the magnetic circuit. It can be concluded that the machines operate at a high saturation level at its rated current.

For these 3 configurations, the same number of turns per coil N_{turns}=160 is used. The flux per phase and phase back EMF at no-load condition are presented in Figures 12a and 12b. Comparing to DSPM0, a greater magnetic flux is obtained in DSPM1 and DSPM2. As result they provide higher back electromotive forces. At 50 rpm, RMS values of back-EMFs per phase for DSPM0, DSPM1 and DSPM2 are 129V, 174V and 220V respectively.

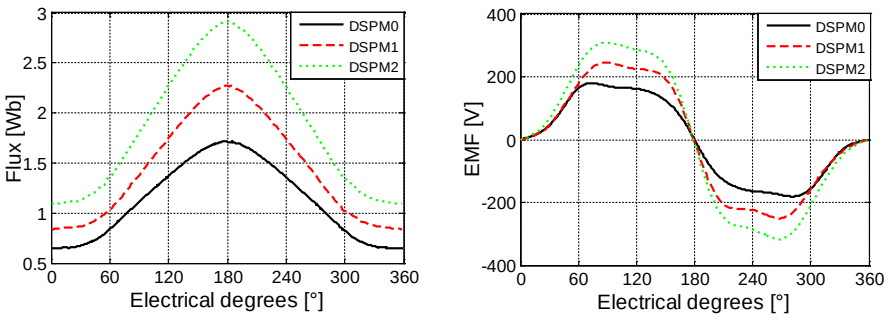

(a) *(b)*

Figure 12. No-load flux and back-EMF per phase of the 3 configurations

The static torque is calculated by the virtual work principle (variation of the co-energy over an electrical period) for a fixed current density Js=5A/mm². Figure 13a shows the static torques corresponding to a single supplied phase, while Figure 13b shows the total torques produced by the 3 phases with "one-phase-on" supply strategy (only one phase is supplied during 120 electrical degrees per period).

As seen in Figure 13b, the torque ripple is significant and taking into account this criterion will be a track for future developments of this work.

The self-inductances per phase are calculated for two values of current density: J_s=0.1A/mm² (Figure 14a) and J_s=5A/mm² (Figure 14b) corresponding to two load conditions. The calculation of inductance consists of subtracting the flux created by the magnets alone, from the total flux under excitation of both the magnets and the current in the phase winding (Ming *et al.*, 2001b; Harkati *et al.*, 2013).

Armature reaction will affect the level of saturation for each machine which is more remarkable on the self-inductances variations of DSPM0 and DSPM1. The level of saturation for DSPM2 varies slightly, so it can be concluded that for DSPM2, the saturation level relates mainly to the permanent magnets flux and is only slightly affected by the value of the current.

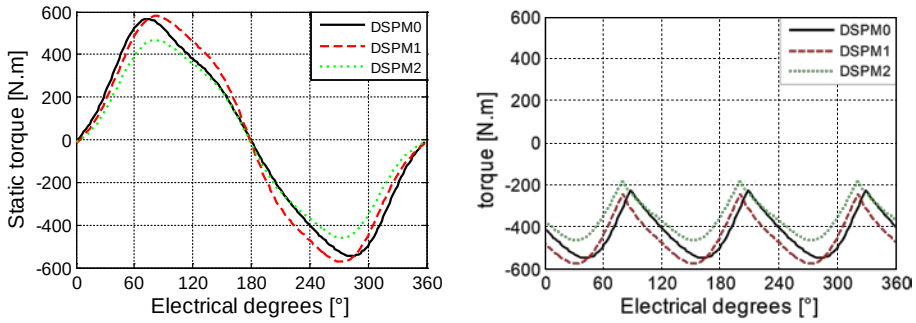

(a) *(b)*

Figure 13. Static torque per phase and the three-phase torque of the 3 configurations at full load

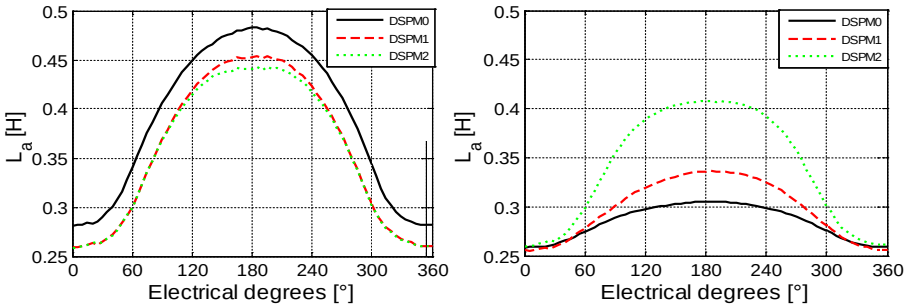

(a) J_s*=0.1 A/mm²* *(b)* J_s*=5 A/mm²*

Figure 14. Self-inductance per phase of the 3 configurations

Flux *vs.* current characteristics of the 3 configurations are presented in Figure 15. These 3 machines have different shape and dimensions of the stator slots. This is why with a fixed maximal current density in the coils (5A/mm²) and the same slot fill factor (k_r=0.5), we obtain different maximum current (9.57A, 9.5A and 7A) for DSPM0, DSPM1 and DSPM2 respectively.

It can be noticed that in the presented study the 3 configurations have been compared considering the same volume. However for a given specifications (power speed), the dimensions of the 3 machines can be adjusted to have the same output power by varying only the length of each machine. To obtain a 2kW machine as for DSPM0, the effective length will be $long_{adj1}$=153.2mm for the DSPM1 and $long_{adj2}$=197.1mm for the DSPM2.

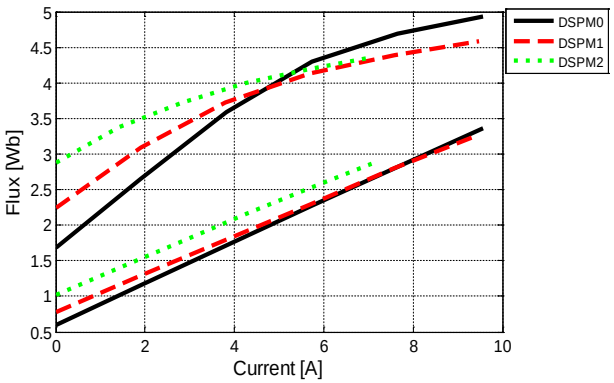

Figure 15. Flux vs. current characteristics of the 3 configurations

Table 4. Selected Configurations Dimensions

Symbol	Quantity	DSPM0	DSPM1	DSPM2
R_c (mm)	Outer radius	200	200	200
long (mm)	Length	150	150	150
e (mm)	Air gap	0.5	0.5	0.5
R_r (mm)	Core radius	152	148.3	149
E_r (mm)	Rotor yoke	16	14.9	17
h (mm)	Teeth height	7	8.4	8
α	Teeth cyclic ratio	0.35	0.32	0.322
H_{PM} (mm)	Magnets width	16	21.5	26.9
E_{PM} (mm)	Magnets width	15	12.3	25.5
β (°)	Slot opening angle	*5*	*3.8*	*3.5*
β_A (°)	Point A angle	*9*	*8.9*	*8.8*

Table 5. Selected configurations characteristics

Symbol	Quantity	DSPM0	DSPM1	DSPM2
λ	Energy ratio	*0.59*	*0.67* *[+14%]*	*0.76* *[+29%]*
Γ_{mass} *(N.m/kg)*	Mass to torque ratio	*6.39*	*6.04* *[-5%]*	*4.66* *[-27%]*
E (V)	RMS back-emf	*129*	*171*	*164*
M_{iron} *(kg)*	Iron mass	*58.8*	*61.7* *[+5%]*	*65.0* *[+10%]*
M_{cu} *(kg)*	Copper mass	*19.6*	*19.5* *[-0.5%]*	*14.6* *[-26%]*
M_{PM}*(kg)*	PM mass	*1.23*	*1.37* *[+11%]*	*3.5* *[+185%]*
M_{tot} *(kg)*	Total mass	*79.6*	*82.6* *[+4%]*	*83.2* *[+5%]*

4. Conclusion

In this study, a design methodology of an unconventional structure for tidal generator called DSPM is proposed. This approach takes into account both the generator compactness and the converter sizing. A criterion called energy ratio is defined to evaluate the generator sizing and simple calculation method of both torque and energy ratio is presented. The influence of geometry dimensions on the design criterions is firstly analysed. Results show that the shape of the teeth constitutes a major parameter because the electromagnetic energy conversion depends on the reluctance variation in the air gap. Results also assess the influences of the PM and slot dimensions on the design criterions.

A systematic design process has been carried out to find a compromise between the maximization of the torque to mass ratio and the minimization of the converter sizing (based on the estimation of energy ratio). This process allows highlighting a Pareto front. 3 configurations of DSPM structure extracted from this Pareto Front are compared in terms of energy ratio, mass to torque ratio and weights of materials used.

To improve the energy ratio, the copper total weight must decrease while increasing the PM weight with almost the same total mass. The PM weight and the converter size have an important impact in cost of the electromechanical conversion chain (generator and converter). The proposed optimization method can be extended to find some interesting compromises between cost and performances.

Bibliography

Benelghali S., Benbouzid M.E.H., Charpentier J.F. (2012). Generator Systems for Marine Current Turbine Applications: A Comparative Study. *Oceanic Engineering, IEEE Journal of*, vol. 37, n° 3, p. 554-563.

Benelghali S.E., Benbouzid M.E.H., Charpentier J.F. (2007). Marine Tidal Current Electric Power Generation Technology: State of the Art and Current Status. *Electric Machines & Drives Conference. IEMDC'07. IEEE International*, vol. 2, p. 407, p. 1412.

Chau K.T., Qiang S., Ying F., Ming C. (2005). Torque ripple minimization of doubly salient permanent-magnet motors. *Energy Conversion, IEEE Transactions on*, vol. 20, n° 2, p. 352-358.

Dinyu Q., Ronghai Q., Lipo T.A. (1999). A novel electric machine employing torque magnification and flux concentration effects. *Industry Applications Conference, 1999. Thirty-Fourth IAS Annual Meeting. Conference Record of the 1999 IEEE*, vol. 1, p. 132-139.

Finite Element Method Magnetics software (FEMM v. 4.2), http://www.femm.info

Harkati N., Moreau L., Zaim M.E., Charpentier J.F. (2013). Low speed doubly salient permanent magnet generator with passive rotor for a tidal current turbine. *Renewable Energy Research and Applications (ICRERA), 2013 International Conference on*, p. 528-533, 20-23.

Jianzhong Z., Ming C., Zhe C., Wei H. (2009). Comparison of Stator-Mounted Permanent-Magnet Machines Based on a General Power Equation. *Energy Conversion, IEEE Transactions on* , vol. 24, n° 4, p. 826-834.

Keysan O., McDonald A.S., Mueller M. (2011). A direct drive permanent magnet generator design for a tidal current turbine(SeaGen). *Electric Machines & Drives Conference (IEMDC), 2011 IEEE International*, p. 224-229, 15-18.

Lawrenson P.J., Stephenson J.M., Blenkinsop P.T., Corda J., Futon N.N. (1980). Variable-speed switched reluctance motors. *Electric Power Applications, IEE Proceedings B*, vol. 127, n° 4, p. 253-265.

Miller T.J.E. (1985). Converter Volt-Ampere Requirements of the Switched Reluctance Motor Drive. *Industry Applications, IEEE Transactions on*, vol. IA-21, n° 5, p. 1136-1144.

Miller T.J.E. (1993). Switched Reluctance Motors And Their Control. *Oxford University Press*, ISBN 9780198593874.

Ming C., Chau K.T., Chan C.C. (2001). Design and analysis of a new doubly salient permanent magnet motor. *Magnetics, IEEE Transactions on* , vol. 37, n° 4, p. 3012-3020.

Ming C., Chau K.T., Chan C.C. (2001). Static characteristics of a new doubly salient permanent magnet motor. *Energy Conversion, IEEE Transactions on* , vol. 16, n° 1, p. 20-25.

Ming C., Wei H., Jianzhong Z., Wenxiang Z. (2011). Overview of Stator-Permanent Magnet Brushless Machines. *Industrial Electronics, IEEE Transactions on* , vol. 58, n° 11, p. 5087-5101.

Pinilla M. (2012). Performance Improvement in a Renewable Energy Direct Drive Permanent Magnet Machine by means of Soft Magnetic Composite Interpoles. *Energy Conversion, IEEE Transactions on,* vol. 27, n° 2, p. 440-448.

Rezzoug A., Zaïm M.E. (2011). Non-conventional Electrical Machines. *Wiley-ISTE*, ISBN 9781848213005.

Sadowski N., Lefevre Y., Lajoie-Mazenc M., Cros J. (1992). Finite element torque calculation in electrical machines while considering the movement. *Magnetics, IEEE Transactions on,* vol. 28, n° 2, p. 1410- 1413.

Saou R., Zaïm M. E., Alitouche K. (2008). Optimal designs and comparison of the doubly salient permanent magnet machine and flux-reversal machine in low-speed applications. *Electric Power Components and Systems,* vol. 36, n° 9, p. 914-931.

Typical data for SURA® M400-50A, https://cogent-power.com

Wang C.X., Boldea I., Nasar Syed A. (2001). Characterization of three phase flux reversal machine as an automotive generator. *Energy Conversion, IEEE Transactions on* , vol. 16, n° 1, p. 74-80.

Wang L., Li C. (2011). Dynamic Stability Analysis of a Tidal Power Generation System Connected to an Onshore Distribution System. *Energy Conversion, IEEE Transactions on,* vol. 26, n° 4, p. 1191-1197.

Wei H., Ming C., Zhu Z.Q., Howe D. (2008). Analysis and Optimization of Back EMF Waveform of a Flux-Switching Permanent Magnet Motor. *Energy Conversion, IEEE Transactions on* , vol. 23, n° 3, p. 727-733.

Ying F., Chau K.T., Cheng M. (2006). A new three-phase doubly salient permanent magnet machine for wind power generation, *Industry Applications, IEEE Transactions on,* vol. 42, n° 1, p. 53-60.

Yu W., Zhiquan D., Xiaolin W. (2012). A Parallel Hybrid Excitation Flux-Switching Generator DC Power System Based on Direct Torque Linear Control. *Energy Conversion, IEEE Transactions on,* vol. 27, n° 2, p. 308-317.

Yuefeng L., Liang F., Lipo T.A. (1995). A novel permanent magnet motor with doubly salient structure. *Industry Applications, IEEE Transactions on* , vol. 31, n° 5, p. 1069-1078.